Published in final edited form as:

Clin Cancer Res. 2021 November 15; 27(22): 6235–6249. doi:10.1158/1078-0432.CCR-21-0971.

FLT3L release by NK cells enhances response to radioimmunotherapy in preclinical models of HNSCC

Thomas E Bickett[1], **Michael Knitz**[1], **Laurel B Darragh**[1], **Shilpa Bhatia**[1], **Benjamin Van Court**[1], **Jacob Gadwa**[1], **Shiv Bhuvane**[1], **Miles Piper**[1], **Diemmy Nguyen**[1], **Hua Tu**[2], **Laurel Lenz**[3], **Eric T Clambey**[4], **Kevin Barry**[5], **Sana D Karam**[1]

[1]Department of Radiation Oncology, University of Colorado, Anschutz Medical Campus, Aurora, CO

[2]Lake Pharma, The Biologics Company, San Francisco, CA

[3]Department of Immunology, University of Colorado, Anschutz Medical Campus, Aurora, CO

[4]Department of Anesthesiology, University of Colorado, Anschutz Medical Campus, Aurora, CO

[5]Immunotherapy Integrated Research Center, Fred Hutchinson Research Institute, Seattle, WA

Abstract

Purpose: Natural Killer (NK) cells are type 1 innate lymphoid cells that are known to secrete cytokines and for their role in killing virally infected cells or cancer cells through direct cytotoxicity. In addition to direct tumor cell killing, NK cells are known to play fundamental roles in the tumor microenvironment through secretion of key cytokines such as FMS-like tyrosine kinase 3 ligand (FLT3L). Although radiation therapy (RT) is the mainstay treatment most cancers, the role of radiation therapy on NK cells is not well characterized.

Experimental Design: This study combines radiation, immunotherapies, genetic mouse models, and antibody depletion experiments to identify the role of NK cells in overcoming resistance to RT in orthotopic models of head and neck squamous cell carcinoma.

Results: We have found that NK cells are a crucial component in the development of an anti-tumor response, as depleting them removes efficacy of the previously successful combination treatment of RT, anti-CD25 and anti-CD137. However, in the absence of NK cells, the effect can be rescued through treatment with FLT3L. But neither RT with FLT3L therapy alone nor RT with anti-NKG2A yields any meaningful tumor growth delay. We also identify a role for IL-2 in activating NK cells to secrete FLT3L. This activity, we show, is mediated through CD122, the intermediate affinity IL-2 receptor and can be targeted with anti-CD25 therapy.

Conclusions: These findings highlight the complexity of using radio-immunotherapies to activate NK cells within the tumor microenvironment, and the importance of NK cells in activating dendritic cells for increased tumor surveillance.

[*]**Corresponding author:** Sana D. Karam, MD, PhD, Department of Radiation Oncology, 1665 Aurora Court Suite 1032, Aurora, CO 80045, Phone: 720-848-0910, Fax: 720-848-0238, sana.karam@cuanschutz.edu.

Data and material availability: All data and materials used in the analysis are available upon request.

Conflict of interests: The authors declare no potential conflicts of interest.

Introduction

Head and Neck Squamous Cell Carcinoma (HNSCC) is a spontaneously arising cancer that affects over 600,000 patients annually (1). For locally advanced disease, chemotherapy and radiation therapy (RT) or surgery and risk-adapted adjuvant chemo-radiotherapy remain the standard of care, with a five-year survival rate of around 50% (1). Clinical trials are currently underway for immunotherapies, but HPV-negative HNSCCs are characterized by low immune cell infiltration, and have exhibited poor response to immunotherapy (2). Preclinical evidence shows a benefit of combination therapies, in which RT is added to immunotherapy to sensitize the tumor microenvironment (TME) to checkpoint inhibition immunotherapies, such as programmed death receptor ligand 1 (PD-L1) (3). Unfortunately, even in this context, the development of adaptive resistance to radioimmunotherapy remains a confounding factor (4,5), and the mechanisms that mediate resistance to combination radioimmunotherapy remain unknown. Many new therapies focus on switching the largely inhibitory immune response found in most HNSCC to a pro-inflammatory one by removing inhibitory signals, such as checkpoint inhibitors (4). However, preclinical evidence suggests that these immunotherapies are ineffective at eliminating resistance to radiation (6,7), and alternate options require further inquiry.

In some mouse models of HPV-negative HNSCC, regulatory T cells (Tregs) have been identified as key regulators of immunosuppression within the TME, and depletion of Tregs through anti-CD25 antibody can lead to tumor eradication (5). However, a variety of cells express CD25, the alpha subunit of the IL-2 receptor, leaving the potential for off target effects. Natural killer (NK) cells are one such population of CD25-expressing cells. In addition to their ability to contribute to killing virally infected or cancerous cells through cytotoxic activity, NK cells are known to regulate the immune response in melanoma through production of FMS-like tyrosine 3 ligand (FLT3L) (8), allowing for expansion of dendritic cells (DCs) in the TME, which increases tumor surveillance and antigen presentation (9,10).

Activating NK cells, as a form of immunotherapy, represents an understudied area with high potential. Monalizumab, a monoclonal antibody targeting the inhibitory receptor NKG2A on NK cells, has previously been proposed as an immunotherapy to activate NK cells (11). However, as we show here, anti-NKG2A antibody fails to activate NK cells in the HNSCC TME, even when combined with RT. For activation by cytokines, NK cells rely on IL-15 (12-14) and to some extent IL-2, although the role or the latter is not completely understood (14,15). The IL-2 receptor is composed of CD25 (IL-2r alpha), CD122 (IL-2r beta), and CD132 (IL-2r gamma). Both the IL-2 and IL-15 receptors are heterotrimeric, and share the same beta and gamma subunits, which could result in overlapping functions (16). There is some evidence that in humans, IL-2 can stimulate $CD25^{+}$ NK cells from the liver to proliferate (17), and studies in multiple sclerosis have identified a role for the intermediate affinity IL-2 receptor, CD122, in IL-2-mediated activation of NK cells (18). Although differences between human and murine NK cells exist, NK cells of mice can also express the IL-2 receptor and respond to IL-2 (19). Our past work has demonstrated success using anti-CD25 antibodies to eliminate resistance to RT in a murine HNSCC model, mostly focusing on the effect of anti-CD25 on T cell and Treg populations. Here,

we show that depletion of NK cells removes efficacy of combination therapy involving RT and anti-CD25. Treatment efficacy can then be restored through FLT3L therapy, which expands DC populations, and allows for increased T cell activity. We show that NK cells become more activated upon anti-CD25 treatment, and this activation is due to increased circulating IL-2. Although anti-CD25 does block IL-2 from activating CD25, we show that IL-2 is able to activate NK cells through binding CD122, the intermediate affinity IL-2 receptor. The novel finding of FLT3-L-mediated interactions between NK cells and DCs in the HNSCC TME suggests that these cell populations will provide key targets for future immunotherapies.

Materials and Methods

RNAseq

Tumors for RNAseq analysis were harvested and immediately frozen in liquid nitrogen. Frozen tumors were stored at −80C until time of analysis. RNA from tumors was extracted using an RNA miniprep kit (Zymo Research, Irvine CA). Sequencing was performed by the genomics core facility at the University of Colorado Denver Cancer Center. RNAseq was performed on a NovaSEQ 6000 with PolyA selection and 2 x 150 paired end reads. Samples were sequenced to a depth of 20 million reads per sample.

Cell lines and cell culture

Murine MOC2 and LY2 squamous cell carcinoma cell lines were used for *in vivo* studies and MOC2 cells were used for *in vitro* studies. The MOC2 cell line (obtained from Dr. Ravindra Uppaluri, Dana-Farber Cancer Institute) was derived from a C57BL/6 mouse that developed SCC after exposure of the oral cavity to DMBA over 25-weeks (20). The LY2 cell line (obtained from the lab of Dr. Nadarajah Vigneswaran, University of Texas Health Science Center, Houston) was derived from lymph node metastases that developed in BALB/c mice after inoculation of PAM 212 squamous cell carcinoma cells (21). Both lines exhibit wildtype expression of TP53 and EGFR. LY2 cells were cultured at 37°C, 5% CO_2 in DMEM-F12 supplemented with 10% FBS and 1% primocin/fungin (InvivoGen, San Diego CA); MOC2 cells were cultured at 37°C, 5% CO_2 in DMEM-F12:IMDM (1:2) supplemented with 10% FBS and 1% primocin/fungin (InvivoGen, San Diego CA), 1.75 μg EGF, 20 μg Hydrocortisone, and 0.1% insulin solution (human) (Sigma Aldrich, St. Louis MO). All cell lines were used within 5 passage of thawing.

Animal Tumor Model

Orthotopic HNSCC models were established as previously described (3). Briefly, cells were mixed at equal volumes with Matrigel (10 mg/mL, BD Biosciences, San Jose, CA), and injected into the buccal mucosa of 6-8 week old mice at a final concentration of 1×10^6/0.1 ml per mouse for LY2 cells and 1×10^5/0.1 ml per mouse for MOC2 cells. BALB/c (Charles River, Wilmington MA) and C57BL/6 (Jax Labs, Bar Harbor ME) mice were used for LY2 and MOC2 cell lines, respectively. Mice with a diphtheria toxin receptor-eGRP gene under control of the FoxP3 promoter, or DEREG mice (22), were obtained through Ed Chan, our collaborator. Mice deficient in the BATF3 gene and lacking DC function (23) were obtained through Jackson labs (#013755). Treatment was started when the average tumor size reached

100-200 mm^3 (8-10 days post inoculation). Tumor size was measured twice weekly with digital calipers, and tumor volumes were estimated using the formula ($V=A\times B^2/2$ mm^3), where A is the longer and B is the shorter diameter of the tumor. Mice exhibiting signs of morbidity according to the guidelines set by the Institutional Animal Care and Use Committee (IACUC) were sacrificed immediately. Primary tumors and regional lymph nodes were harvested upon sacrifice.

Irradiation

Irradiation was performed using the X-RAD SmART image-guided irradiator (Precision X-Ray Inc., Branford CT) at 225 kVp, 20 mA with a 0.3 mm Cu filter. During mouse buccal irradiation, mice were anesthetized with isoflurane and positioned in the prone orientation. A CT scan was acquired prior to radiation delivery (5.6 Gy/min). LY2 tumors were treated with 1 dose of 10 Gy, as this is enough to achieve eradication whereas MOC2 tumors were treated with 3-5 doses of hypofractionated radiation at 8 Gy per dose to achieve eradication as previously reported (24).

Antibody Treatment and Depletions

For antibody depletion experiments, anti-CD25 (Clone: PC-61.5.3, Bio X Cell, Lebanon NH), anti-CD4 (Clone:GK1.5, Bio X Cell, Lebanon NH), anti-CD8a (Clone:53-6.7, Bio X Cell, Lebanon NH), anti-CD137 (4-1BB, Clone:3H3, Bio X Cell, Lebanon NH) were injected (i.p.) at 10 mg/kg/dose twice weekly for the length of each experiment. All antibody-based treatments were accompanied by the isotype controls at the same dose, and in the same time frame. Diphtheria toxin (DT) was administered twice weekly (i.p.) to DEREG mice at a dose of 1 μg/mouse as previously reported (25).

Flow cytometry in vitro and in vivo procedures

For flow cytometric analysis of tumor tissue, single-cell suspensions of tumor cells were prepared as previously described (26). Briefly, tumors were minced, and placed in HBSS solution containing 200 U Collagenase III (Worthington, Lakewood NJ) for 40 minutes at 37°C with gentle shaking every 15 minutes. After the incubation period, tumor pieces were passed through a 70 μm nylon mesh. The resulting cell suspension was centrifuged and re-suspended in red blood cell lysis buffer for 5 minutes (InVitrogen, Carlsbad CA). HBSS was added to inactivate RBC lysis buffer, cell suspensions were centrifuged, re-suspended, and counted using an automated cell counter. Draining lymph nodes were also collected where described, and were processed into single-cell suspensions through mechanical separation. For intracellular flow cytometric analysis, 2×10^6 live cells were plated in 24-well plates and cultured for 4 hours in the presence of monensin to prevent release of cytokines; PMA and ionomycin were added to cultures to stimulate cytokine production. After the incubation period, cells were incubated with the live/dead aqua viability stain kit (Invitrogen, Carlsbad CA) for 30 min at 4°C. Cells were centrifuged, and then incubated with FC block (anti-CD16/32 antibody) (Tonbo Biosciences, San Diego CA) for 20 min at 4°C. Cells were centrifuged, and then resuspended in buffer containing staining antibodies, and incubated at 4°C for 20 min. For analysis of immune cells, the following conjugated antibodies were used: PerCP-CD45 (Clone: 30-F11, BD Biosciences, La Jolla CA), BUV395-CD3 (Clone: 145-2C11, BD Biosciences, La Jolla CA), PercP-Cy5.5-CD3 (Clone: 145-2C11,

BD Biosciences La Jolla CA) SuperBright436-CD4 (Clone: GK1.5, Invitrogen, Carlsbad CA), BrilliantBlue515-CD8 (Clone: 53-6.7, BD Biosciences, La Jolla CA), PE-FoxP3 (clone: MF-14, Biolegend, San Diego CA), AF488-FoxP3 (Clone: MF-14, Biolegend, San Diego CA), FITC-FoxP3 (Clone: 3G3, Millipore/Sigma, Burlington MA), BV605 IFN-γ (Clone: B27, BD Biosciences La Jolla CA), BV421-IFN-γ (Clone: B27, BD Biosciences, La Jolla CA), efluor450-TNF- α (Clone: MP6-XT22, Invitrogen, Carlsbad CA), BV750 TNF-α (Clone: MP6-XT22, BD Biosciences, La Jolla CA), PE-Cy7- NK1.1 (Clone: PK136, BD Biosciences, La Jolla CA), FITC-Granzyme-B (Clone: GB11, BD Biosciences, La Jolla CA), BUV737-CD11b (Clone: M1/70, BD Biosciences, La Jolla CA), APC-CD11c (Clone: HL3, BD Biosciences, La Jolla CA), APC-Cy7-F4/80 (Clone: BM8, Biolegend, San Diego CA), PE-Dazzle594-CD103 (Clone: 2E7, Biolegend San Diego CA), BV650-I-Ab (Clone: M5/114, BD Biosciences, La Jolla CA), BV480-CD80 (Clone: 16-10A1, BD Biosciences, La Jolla CA), PercP-efluor710-PD-L1 (Clone: MIH5, ebiosciences San Diego, CA) efluor450-Ly6C (Clone: HK1.4, Invitrogen, Carlsbad CA), BV785-Ly6G (Clone: 1A8, BD Biosciences, La Jolla CA), Brilliantblue700- PD-1 (Clone: RMP1-30, BD Biosciences, La Jolla CA), PE-Perforin (Clone: S16009A, Biolegend San Diego CA), BV421-CD25 (Clone: 3C7, BD Biosciences, La Jolla CA), BV480-CD27 (Clone: LG3A10, BD Biosciences, La Jolla CA), PECy7-NKp46 (Clone: 29A1.4, Biolegend San Diego CA), efluor-450 CD122 (Clone TM-b1, ebioscience, San Diego CA), BV711-CD314 (NKG2D) (Clone: CX5, BD Biosciences, La Jolla CA), BV786-LY49A (Clone: A1, BD Biosciences, La Jolla CA), Alexa Fluor 647-LY49H (Clone: CD10, BD Biosciences, La Jolla CA), BV605-DNAM-1 (CD226) (Clone: 10E5, BD Biosciences, La Jolla CA). Flow cytometry samples were analyzed on an Aurora spectral cytometer (Cytek Biosciences, Fremont CA) at the University of Colorado Denver Cancer Flow Cytometry Core. Fluorescence minus-one (FMO) controls were used to determine gating. Data were analyzed using FlowJo Analysis software (Flowjo, Ashland OR).

FLT3L HDT and IP injection

FLT3L was administered either by i.p. injection of 10 μg/mouse, or by hydrodynamic delivery (HDT) via tail vein of 10 μg FLT3L plasmid (LakePharma, San Francisco, CA) dissolved in 1.5 mL dPBS.

Serum ELISA and supernatant ELISA for IL-2 and FLT3L

Blood samples from living animals were collected by cheek punch from mice at specified time points. Terminal bleeds were taken via heart stick upon sacrifice. Serum was obtained from blood samples collected in BD microtainers (BD Biosciences, San Jose CA) following incubation for 30 min at room temperature and centrifugation at 6000 RPM for 2 minutes. Collected serum was stored at-80°C until time of analysis.

FlowSOM

FlowSOM (self-organized map) analysis was conducted using a previously published protocol (27) following initial data collection using FlowJo. Live cells from singlets gate were identified using viability dye 510 (Invitrogen, Carlsbad CA). NK cells were selectively gated based on expression of CD45 and NKp46. All samples were concatenated into a single file, and were then run through the Phenograph plugins available in FlowJo using

the compensated parameters for the markers indicated in each heat map. Initial analysis with Phenograph identified the number of potential clusters. The concatenated file was then run through FlowSOM using the number of meta clusters identified by Phenograph and indicated in the heatmaps. The same analysis was subsequently performed on the individual treatment groups and results were mapped to the first tree, ensuring comparability between results. Heatmaps were generated using R studio.

In vitro NK cell killing assay

Calcein release killing assay was performed as described previously (28). Briefly, NK cells were isolated from naïve C57BL/6 mouse spleens with an NK cell negative selection isolation kit (Miltenyi biotec, Bergisch Gladbach). Target cells, MOC2 tumor cells, were stained with Calcein (ThermoFisher, Waltham MA) in a 2 μg/mL solution in RPMI media with 10% FBS. NK cells were incubated with target cells at an effector:target ratio of 2:1. Stimulation was added as indicated at the following concentrations: IL-2, 1000 U/mL (29), IL-15, 20 ng/mL (29), IL-15 SA, 50 ng/mL (30), anti-CD25, 10 mg/mL. IL-15SA was created by mixing 0.75 μg rIL-15 (ebioscience) with 7 μg rIL-15RA-FC chimera protein (R&D systems), and incubating for 30 mins at 37°C. Stimulants were added to cultures and incubated for 4 hours. Plates were centrifuged, and supernatant was removed to a flat bottom plate. Fluorescence was read on Tecan Infinite M plex fluorescence plate reader and 485 nm/530 nm ratio was calculated. Specific cell lysis was calculated through the equation: (Test release−Spontaneous release)/(Maximum release−Spontaneous release)] ×100. Maximum release was calculated following incubation of target cells with 1% triton X in media, and spontaneous release was calculated following incubation of target cells in 10% RPMI with no stimulus.

Immunoprecipitation and Western Blot

NK cells were isolated from C57BL/6 mouse spleens with an NK cell negative selection isolation kit (Miltenyi biotec, Bergisch Gladbach). Cells were suspended in 1× Cell Lysis Buffer containing protease and phosphatase inhibitors. Lysate was diluted to 1 μg/μL in lysis buffer, and 100 μL of the diluted lysate was incubated with anti-CD122 antibody (Santa Cruz Biotechnologies, Dallas TX) at a 1:100 dilution overnight at 4°C with end-over-end rotation. Magnetic protein G beads (Bio-Rad) were washed three times with 1× PBS, added to lysate–antibody complexes, and the mixture was incubated overnight at 4°C with end-over-end rotation. Beads were washed three times with cold 1:1 lysis buffer:PBS, removing supernatant after each wash. Protein was eluted from beads by adding 1× sample loading buffer (Invitrogen) containing reducing agent (Invitrogen), and boiling beads at 95°C for 15 minutes. A total of 100 μg equivalent starting material was resolved on a 10% SDS-PAGE gel, and then transferred to Immuno-Blot PVDF membrane (Bio-Rad). Membranes were probed for total phosphotyrosine using anti-phosphotyrosin 4G10 (Cell Signaling Technology).

Survival Curves and pathway analysis

Survival curves were generated with UCSC Xena browser at xenabrowser.net using the TCGA Head and Neck Cancer (HNSC) dataset. Phenotypic sample type was chosen and samples with primary tumor were used. High expression of FLT3 and FLT3LG was

determined by Log2 transformed normalized expression with a threshold of 3.463 for FLT3 and 7.13 for FLT3LG. Gene set enrichment analysis was performed differential expression function within the Xena browser. Gene set enrichment analysis was performed using the full ranked list of genes by log2 fold change for the indicated comparisons using the fgsea R package (31) on KEGG pathways (32). Waterfall plots of pathways were created in R.

Statistical analysis

Statistical analysis was completed using one-way ANOVA with Tukey correction for all comparisons with three or more groups, and unpaired t-tests were used for all comparisons involving two groups; other tests were used where indicated. All statistical analyses were performed in Prism software (GraphPad, v8.00). All statistical tests were two-sided. Box and whisker plots illustrate mean with standard deviation noted by error bars. For studies involving tumor growth curves, data points represent repeat measurements of individual tumors at indicated time points. All other graphs represent measurements taken from distinct samples.

Study Approval

All protocols for animal tumor models were approved by the IACUC of the University of Colorado, Denver.

Model creation

Figure 6 was created through Biorender.com.

Results

Anti-NKG2A antibody in combination with radiation increases intratumoral DC recruitment but fails to enhance DC or Teff activation leading to sustained tumor growth

Tumor-associated NK cells from primary human HNSCCs have been shown to upregulate the inhibitory receptor NK group 2 member A (NKG2A) (33). We, therefore, sought to test the hypothesis that therapeutic resistance to RT in HPV-negative models of HNSCCs could be overcome by targeting NKG2A. Monalizumab, a monoclonal antibody that targets the NKG2A receptor on both CD8 T cells and NK cells, has shown enhanced NK cell cytotoxicity when combined with anti-EGFR antibodies (11). In mice, NKG2A binds to the receptor Qa-1^b (34), which remained highly expressed both before and after RT (Figure 1A). Expression of NKG2A did not change in relation to RT as well (supplementary Figure 1A). We hypothesized that this could lead to a synergy between RT and anti-NKG2A. In combination with RT, however, neither MOC2 nor LY2 tumors showed a significant response to anti-NKG2A (Figure 1B). Depleting NK cells with anti-NK1.1 and anti-Asialo GM1 also had no effect on the lack of response to anti-NKG2A (Figure 1B) suggesting that any effect induced by anti-NKG2A was unaffected by the presence or absence of NK cells.

Flow cytometric analysis indicated that blocking NKG2A failed to enhance NK cell recruitment or expression of IFNγ or Granzyme B in the MOC2 model (Figure 1C), and did not affect NK populations defined by NK cell developmental markers $CD27^{hi}$ $CD11b^{lo}$ (terminal) or $CD27^{lo}$ $CD11b^{hi}$ (naïve) (Supplemental Figure 1B) (35). However,

NK cell depletion during RT or combination RT and anti-NKG2A therapy resulted in three significant findings. First, we observed a significant increase in intratumoral FoxP3$^+$ Tregs, known to be immunosuppressive, with NK cell depletion and RT and anti-NKG2A therapy (Supplementary Figure 1C). Second, while we observed a significant increase in intratumoral CD11c$^+$ CD103$^+$ DCs (Figure 1D), no change in lymph node CD103$^+$ DCs or serum FLT3 was detected, suggesting no increase in antigen presentation (Figure 1D). And, third, the RT and anti-NKG2A combination was not associated with an increase in effector T cells as measured by Granzyme B production by CD8 T cells or IFNγ production by CD4 T cells (Figure 1E).

With these results, we hypothesized that while anti-NKG2A antibody with RT did stimulate DC recruitment, recruited DCs were unable to override the negative effects of FoxP3$^+$ Tregs still present within the tumor (Supplementary Figure 1B). Additionally, whereas anti-NKG2A has shown a propensity to increase the cytolytic effect of NK cells (11), DCs in lymph node and T cells in tumor remain unchanged. However, the addition of anti-NKG2A to our previously successful triple combinational therapy of RT, anti-CD25 antibody to deplete Tregs, and anti-CD137 antibody to activate DCs (24) failed to confer additional benefits in the MOC2 model (Supplementary Figure 1D) suggesting that any benefit of cell activation from anti-NKG2A is not unique, and can be attained through other means.

NK cells and FLT3L are a necessary requirement for successful combination radioimmunotherapy

With the failure of blocking NKG2A to activate NK cells, we sought other approaches. Our previous work has shown that, unlike the LY2 tumor model, Treg depletion with anti-CD25 combined with RT is not sufficient to overcome radioresistance in the MOC2 tumor model (5). Based on the above findings and our previous data (24), we hypothesized that activation of the DCs would be required to overcome resistance in immunologically cold tumors in the context of RT. Previous studies in B16 melanoma models have indicated that NK cells are required for successful activation of DCs via anti-CD137 immunotherapy (36). This caused us to question the role of NK cells in DC activation in our HNSCC tumor models. We had previously shown that combination therapy with RT, anti-CD25, and anti-CD137 antibodies significantly delayed tumor growth in the MOC2 tumor model (24), and RT and anti-CD25 doublet therapy did the same in the LY2 tumor model (5). Our previous analysis showed sustained activation of DC populations upon treatment with a combination of RT, anti-CD25, and anti-CD137 in the MOC2 tumor model, and here we observed trending DC activation within the tumor and small increases in the blood of mice treated with RT + anti-CD25 in the LY2 model (Supplementary Figure 2A). RNAseq analysis showed that that IL-15, IL-2, IL-2RA, and IL-2RB production remain unchanged after RT in both MOC2 and LY2 models, suggesting that NK cells lack sufficient activating cytokines with RT alone treatment (Figure 2A, B). Similarly, FLT3L RNA also remains low, suggesting that DCs lack continued growth factor signals (Figure 2A, B). Thus, we hypothesized that expansion and activation of DCs through FLT3L therapy, as seen previously (37), would eliminate resistance in the context of RT. Unexpectedly, the use of FLT3L therapy to activate DCs in conjunction with RT was insufficient to prevent resistance to RT (Figure 2C). This suggests

that expansion of DCs alone is unable to overcome resistance to RT, and involvement of other cell types is necessary.

In a series of loss of function and rescue of function experiments, we sought to determine the necessity of NK cells for production of FLT3L to impart a tumor growth inhibiting effect of radioimmunotherapy in our MOC2 non-T cell inflamed tumor model (Figure 2D). NK cell depletion with anti-NK1.1 eliminated the effect of the combined RT, anti-CD137, and anti-CD25 therapy (Figure 2E). Addition of FLT3L therapy after NK cell depletion rescued the effect of the triple therapy (Figure 2E). Similarly, NK cell depletion by anti-Asialo GM1 in LY2 tumors (Figure 2F) eliminated the beneficial effect of combined RT + anti-CD25 therapy (38) (Figure 2G). Rescue of function with FLT3L therapy also restored the response to RT+anti-CD25 in the LY2 tumor model after NK cell depletion. This result was supported by serum analysis, which showed a significant decrease in FLT3L with NK cell depletion, and restored levels in the NK-depleted groups treated with FLT3L at 8 days post RT (supplementary Figure 2B). It should be noted that no difference was recorded in nodal metastasis between these groups. To confirm the role of FLT3L in RT + anti-CD25 + anti-CD137 therapy, we used a FLT3L KO mouse (C57BL/6 background). FLT3L KO mice treated with RT + anti-CD25 + anti-CD137 showed no tumor growth delay compared with WT mice (Figure 2H). This suggests that the effect of therapy is dependent on FLT3L. Overall these data support our hypothesis that expansion of DCs alone is not sufficient to eliminate resistance to RT, and other signals are necessary for a successful immune response.

FLT3L produced by NK cells is required for DC tumor surveillance and CD8 T cell activation

With the understanding that stimulation of NK cells and DCs is required to overcome resistance to RT, we hypothesized that DCs mediate CD8 T cell cytotoxicity in the TME. Previous reports detailing the importance of interactions between NK cells and DCs in melanoma have highlighted the significance of $CD103^+$ DC populations to proper antigen presentation (8,39). In order to continue use of FLT3L we employed hydrodynamic delivery of the pLEV mammalian expression vector. Through testing the vehicle control and FLT3L pLEV vector we determined that vector expressed FLT3L was sufficient to inhibit tumor growth (supplementary figure 3A). In both our MOC2 and LY2 models of the HNSCC TME, we found that there was an increase in numbers of $CD103^+$ DCs after FLT3L therapy (Figure 3A). We previously showed that $CD103^+$ DCs are required for efficacy of treatment with RT, anti-CD25, and anti-CD137 therapy, and this triple combination radioimmunotherapy increased DC trafficking to lymph nodes (24). We have also previously reported the activating effect of this triple combination radioimmunotherapy on T cell populations (24), and here we confirm that FLT3L therapy acts further to stimulate CD8 T cell populations within the TME (Figure 3B). To test the dependence of the FLT3L rescue response to radioimmunotherapy on T cells or DCs, we conducted pharmacologic and/or genetic depletion experiments in which animals received the triple combination RT, NK, FLT3L therapy (Figure 3C). Antibody depletion of CD8 T cells, and genetic depletion through $RAG^{-/-}$ KO mice removed any rescue effect of FLT3L therapy (Figure

3D), whereas depletion of CD4 T cells did not. This is similar to previous data we have published showing the dependence of the LY2 model on CD4 and CD8 T cells (3,38).

DC and NK cell activating Cytokines in serum were at normal levels, revealing the only difference to be the depleted T cell populations (Figure 3E). This suggests that FLT3L functions through promoting DC-CD8T cell interactions. To assess the role of DCs in TME surveillance and activation during FLT3L therapy, we utilized a BATF3 KO mouse model lacking functional DCs (39) according to the protocol outlined in Figure 3F. Just as in the T cell depletion, mice devoid of DCs showed no rescue of function with NK cell depletion and FLT3L therapy (Figure 3G). Serum levels of FLT3L in treated groups of BATF3 KO mice confirmed elevation of FLT3L (Figure 3H).

To further understand the mechanisms behind FLT3L-mediated tumor clearance, we analyzed the TME after RT. We hypothesized that the FLT3L-induced expansion of DCs resulted in increased T cell activation within the tumor. Our analysis showed that overall CD4 T cell populations were relatively unchanged, but $CD25^{+}$ CD4 T cells were markedly reduced (Figure 3I). We also found that CD4 T cell populations were devoid of any IFNγ (Figure 3I). Importantly, we also found that CD8 T cells were significantly reduced in the tumors of $BATF3^{-/-}$ mice even with FLT3L therapy (Figure 3I), suggesting significantly reduced T cell activation. When looking at an earlier time point, just 3 days after the initiation of FLT3L therapy, we found an increase in Ki67 in CD8 T cells in the lymph node but not in the tumor (Supplementary Figure 3B). This suggests that FLT3L-induced expansion of DCs results in an increase in DC trafficking to the draining lymph nodes, where DC priming of T cells results in an increase in CD8T cell activation.

Anti-CD25 therapy results in activation of circulating and tumor NK cells

The requirement of NK cells for effective anti-CD25 therapy led us to examine the effect of RT combined with anti-CD25 on circulating NK cells and on NKs in the TME. In the MOC2 model, our data showed that NK cells were recruited into the tumor and activated by our triple combination radioimmunotherapy as reflected by an increase in NK cell IFNγ and a transient increase in TNFα production (Figure 4A, Supplementary Figure 4A). However, no differences were noted between populations of $CD27^{lo}$ $CD11b^{hi}$ (naive) and $CD11b^{lo}$ $CD27^{hi}$ (terminal) NK cells (Supplementary Figure 4B) (35). To better visualize the changes in NK cell populations within the TME after RT + anti-CD25 therapy, we utilized Phenograph and FlowSOM, clustering algorithms to identify unique populations and create self-organized maps. These populations were then characterized through marker expression visualized with heatmaps based on the mean fluorescence intensity (MFI) of each marker. The frequency of each population was then plotted. Within LY2 tumors, we noticed an increase in the presence of NK cells producing IFNγ and TNFα (populations 2 and 7, Figure 4B) similar to our observations with triple therapy in the MOC2 model. A significant increase in NK cell activation in the peripheral blood was also identified through increases in CD27 and NKG2D expression, along with increased production of IFNγ (Figure 4C). This finding was corroborated in MOC2 bearing C57BL/6 mice, as flowSOM revealed populations of TNFα and IFNγ producing NK cells within the tumor when anti-CD25 was added to RT and anti-CD137 therapy (Populations 5, 6, Figure 4D). In addition, populations

expressing high levels of PD-L1 were markedly reduced upon treatment with anti-CD25 (populations 3, 4, 15, 16, and 17, Figure 4D) suggesting further activation of NK cells (40). NK cells found in the blood of the same mice showed significant increases in DNAM1, CD27, TNF-α and LY49H, markers, all suggestive of increased activation (35,41) (Figure 4E). These data indicate that anti-CD25 activates both systemic and tumor NK cells.

Anti-CD25 therapy-mediated Treg depletion allows for increased NK cell activation

As IL-2 and CD25 are key regulators of T cell homeostasis (42), we sought to assess changes to CD4 T cell populations upon anti-CD25 treatment. We found that $CD4^+$ $CD25^+$ T cells were significantly reduced with anti-CD25 treatment (Supplementary Figure 4C). We hypothesized that the $CD4^+$ $CD25^+$ T cells were Tregs, and their removal allowed for increased NK cell activation; we sought to test this in a DEREG mouse model, in which the FoxP3 promoter is under the control of a diphtheria toxin receptor. This model enabled us to interrogate whether anti-CD25 antibody contributed any additional benefit not mediated by $FoxP3^+$ Treg depletion. We found that mice treated with RT and DT to deplete their Tregs, and with anti-CD137 showed modest reductions in tumor growth compared to historical MOC2 tumor experiments. However, tumor sizes were further decreased by the addition of anti-CD25 (Figure 4F). This suggests that anti-CD25 does more than deplete Tregs. We also found an increase in serum FLT3L in DT Treg-depleted and anti-CD25-treated mice (Supplementary Figure 4D), suggesting that immune suppression by Tregs also reduces FLT3L production. Past flow cytometry studies have identified that Tregs are indeed depleted upon addition of DT (24). Here, flow cytometry of tumors in the DEREG model revealed that NK cell population frequencies were unchanged in our treatment groups, but more NK cells expressed CD27 and DNAM-1, suggesting increased activation in the TME (Figure 4G).

To further understand the effect of treatment plus Treg depletion on NK cells we again used Phenograph and FlowSOM. From our analysis, we characterized 14 distinct populations of NK cells. Most of these populations were similar among treatment groups, and expressed similar levels of markers (Figure 4H). However, population 9, was present only when Tregs were depleted with DT. This population is positive for CD25 and CD122 and exhibits high expression of NKG2D, an activating NK cell receptor (Figure 4H, I). The presence of this population was increased upon treatment with anti-CD25 and depletion of Tregs with DT (Figure 4H, I). Additionally, population 3, with expression of other activating markers like NKG2D and DNAM-1, increased in abundance, and population 4, without activation markers decreased in abundance (Figure 4H, I). Overall these data support a model in which anti-CD25 antibody modulates NK cell activation through depletion of $CD25^+$ $CD4^+$ T cells, but which are not necessarily $FoxP3^+$ Tregs.

IL-2 stimulates NK cells through CD122, the intermediate affinity IL-2 receptor

A remaining question is the mechanism by which removal of $CD25^+$ $CD4^+$ T cells activates NK cells. Previous reports using anti-CD25 antibodies have identified IL-2 as an activator of NK cells (18), and we hypothesized that depletion of $CD25^+$ $CD4^+$ T cells would provide similar stimulus. As these mice were treated with anti-CD25, the alpha chain of the IL-2 receptor, it seemed unlikely that IL-2 would be able to stimulate NK cells because the

antibody would be in competition for the receptor. However, CD122, the beta chain of the IL-2 receptor, has been identified as key for activation of NK cells by IL-2 (18). We, therefore, hypothesized that removal of $CD4^+$ $CD25^+$ T cells would reduce IL-2 scavenging, allowing for increased IL-2 availability, and that CD122 was responsible for IL-2-mediated NK cell activation in our model.

We utilized an *in vitro* system to explore activation of NK cells by IL-2 with and without anti-CD25 antibody. As positive controls, we also used IL-15 and IL-15 superagonist (IL-15SA) which are known to activate NK cells (43,44). We found that anti-CD25 antibody did not inhibit IL-2 induced NK cell killing of cancer cells (Figure 5A). Flow cytometry of the *in vitro* stimulated NK cell populations revealed increased secretion of IFNγ and Granzyme B when subjected to IL-2 treatment even when anti-CD25 was added (Figure 5B). Our flow cytometry also revealed that upon IL-2 stimulation, expression of CD122 was markedly reduced (Figure 5C). We hypothesize this was due to internalization and lysosomal degradation of CD122 upon binding with IL-2 (45). Finally, IL-2 consumption by NK cell populations increased when anti-CD25 was used (Figure 5D), suggesting that IL-2 can stimulate NK cells even when the receptor is blocked by anti-CD25 antibody. To confirm this, we immunoprecipitated CD122 from the lysate of NK cells stimulated with IL-2, anti-CD25, or both, and performed a western blot for phospho-tyrosine to assess activation of the receptor. We found that only after addition of both anti-CD25 and IL-2 did we visualize any phosphorylated CD122 (Figure 5E), suggesting activation of this receptor by IL-2 when anti-CD25 was blocked. To corroborate this *in vivo*, we analyzed serum IL-2 of triple combination radioimmunotherapy treated mice, and we found that there was an increase in serum IL-2 following RT, anti-CD25, and anti-CD137 administration (Figure 5F), which would be available to activate NK cells. As the NK cells in blood were activated (Figure 4B and C), this supports our hypothesis that IL-2 drives activation of NK cells in these mice.

Based on these data, we hypothesized that these IL-2 activated NK cells produce FLT3L, which expands DCs leading to a durable CD8T cell response and tumor eradication. Again, our *in vitro* model revealed that IL-2 stimulated NK cells to produce FLT3L (Figure 5G). However, our analysis of DCs after RT and anti-CD25 therapy without anti-CD137 failed to show any meaningful change in activation or expansion (Supplementary Figure 5B). Therefore, to derive the maximal benefit of anti-CD25, we combined it with FLT3L therapy. In our MOC2 model we found that RT + anti-CD25 + FLT3L therapy led to significant tumor growth delay (Figure 5H, Supplementary Figure 5C) confirming that activation of NK cells and DCs is a viable option for overcoming resistance to RT.

FLT3 and FLT3LG correlate with increased survival in human HNSCC

To better understand the role of FLT3L (FLT3LG) in human cancers, we mined the head and neck cancer database from the TCGA. Our initial analysis showed increased 5-year overall survival of patients with increased expression of both receptor and ligand, FLT3 and FLT3LG (supplementary figure 6 A, B). Analysis of a subset of patients with above median expression of both FLT3 and FLT3LG showed improved overall survival compared to those with levels below median levels (Figure 6A). Gene set enrichment analysis of

the top 15 KEGG enriched pathways (32) in this subset of patients with increased FLT3/FLT3LG expression showed enrichment of antigen processing and presentation, T cell receptor signaling, and NK cell mediated cytotoxicity (Figure 6B). These data emphasize the importance of FLT3/FLT3LG expression in human HNSCC and suggest that therapies aimed at enhancing expression of FLT3/FLT3LG may improve survival.

Discussion

Our previous work highlighted how the interaction of DCs and Tregs can be modulated through the use of anti-CD137 antibody (24). Here, we identify NK cells as critical components mediating this cross talk. With reduced IL-2 scavenging by $CD25^+$ $CD4^+$ T cells, more IL-2 is left to activate NK cells. NK cell activation by IL-2 leads to increased production of FLT3L and further DC activation for tumor surveillance and CD8 T cell activation in draining lymph nodes (Figure 6C). As we have shown, each of these components plays a significant role, as depletion of NK cells or DCs or the presence of Tregs abrogates the effects of combination radioimmunotherapy in both the MOC2 and LY2 models. We find that the presence of NK cells is crucial for proper functioning of the anti-CD25 antibody, even within the LY2 model where previously the role of CD25 was thought to be through Treg depletion (24). It is important to note, however, that while FLT3L therapy can activate DCs in place of NK cells, concordant with previously published work in other tumor models (8), in the HNSCC TME, anti-CD25 is still necessary. Combination of RT with FLT3L alone was simply not sufficient in reducing tumor size. This suggests that anti-CD25 has roles other than elimination of IL-2-sequestering T cells. Depletion of Tregs may be crucial to FLT3L efficacy, as T cell responses are clearly involved. Overall, our data suggest a system in which multiple components must cooperate for effective therapy.

A critical piece of evidence emerged from differences noted between the MOC2 and LY2 tumor models. This and previous work have shown that elimination of resistance to RT is possible in the LY2 model through depletion of Tregs (5,24) thereby removing the inhibition on NK cells and T effector functions. In the MOC2 tumor model, however, Treg depletion was essential but not sufficient as this model is more heavily reliant on immunotherapy-mediated DC activation (24). DCs provide important functions within the LY2 TME, but a-CD25 alone appears to be sufficient there in modulating both Tregs and DCs (24). Though it does seem that NK cells are crucial to successful immunotherapy in both models, future studies focused on this aspect may help rectify our understanding of the differences between the MOC2 and LY2 HPV negative HNSCC mouse models.

Our findings are also in line with other studies suggesting that modifying the regulatory capacity of NK cells leads to better anti-tumor responses. Here, we report that NK cell activation by immunotherapy is not important for direct anti-tumor cytotoxic activity, but is important for immunoregulatory activity. Other regulatory roles for NK cells have been identified, such as stimulating memory T cell populations (46) and limiting other aspects of the T cell response through cytokine activity or perforin mediated T cell death (47). Unfortunately, we have little insight into the processes surrounding NK cell immune regulation. IL-2 and CD25 are known to activate immunoregulatory mechanisms in T cell populations (42). $CD25^+$ $CD4^+$ Tregs are known to suppress lymphocyte and NK cell

populations through production of anti-inflammatory cytokines such as TGFβ and IL-10, direct cell-cell interaction, and binding and removal of IL-2 through IL-2 scavenging (42). Our past work has identified the important role of Tregs within LY2 tumors, and has shown that depletion of Tregs with anti-CD25 combined with RT leads to tumor eradication (5). Others have reported that $CD25^{-/-}$ mice lack Tregs, and as a result have elevated amounts of IL-2 in serum (48). Overall, the evidence suggests that depletion of $CD4^{+}CD25^{+}$ T cells may have an indirect role in the activation of NK cells by circulating IL-2.

As we have shown, IL-2 is capable of activating NK cells in mice, and there is the potential that IL-2 also activates the immunoregulatory activities of NK cells. NK cells have been linked to efficacy of anti-CD25 therapy in humans during treatment of multiple sclerosis (49). This has led to the paradoxical finding that in the presence of IL-2 binding to NK cells, blocking CD25 leads to greater activation of NK cells during treatment for multiple sclerosis. (18). Here, we noticed the paradoxical activity of the IL-2 receptor chains in mice, but in light of published studies, our findings suggest the potential for translational crossover to humans during treatment of cancers with anti-CD25 antibodies. We suggest that a major role of anti-CD25 antibody is blocking CD25 on NK cells, thereby forcing IL-2 signaling through CD122, the intermediate receptor. Our data show that *in vitro* IL-2 can stimulate the production of FLT3L by NK cells when CD25 is blocked with antibody. This suggests that the intermediate affinity IL-2 receptor of NK cells is a potential therapeutic target.

Although this is the first time we have achieved durable eradication in the MOC2 tumor model, these results come with limitations. Both the MOC2 and LY2 tumor models are transplanted tumor models, grown first in tissue culture. As Wisdom et al. have shown, transplanted models can respond better to RT and checkpoint inhibitor therapies than autochthonous tumors (50). Importantly, they note that both primary and implant tumors undergo remodeling of the myeloid compartment upon RT suggesting that the DC populations we have targeted here would respond similarly in both primary and implanted tumors. Additionally, the MOC2 model, although a transplanted model, does not respond to checkpoint inhibitors combined with RT making it more difficult to compare the results of this past work. Likewise, work from Crittenden et al. have identified a specific role for pre-existing immunity in transplant models (51). While this is an important factor to consider, again the MOC2 model is an incredibly cold tumor with low T cell infiltration that shows no response to RT and checkpoint inhibition. We have demonstrated here that our combination therapy is able to increase DC activity, tumor surveillance, and T cell activation which would be beneficial to any immunologically cold tumor regardless of pre-existing immunity. As a final comment, using these models has allowed us to study the TME in the buccal mucosa, which better represents the TME of HNSCC patients, and suggests that FLT3L, which has shown promise in clinical trials with melanoma, will translate to HNSCC. This is supported by our data from the TCGA showing increased survival in patients with higher FLT3/FLT3LG expression, which also resulted in increased T cell receptor signaling and antigen presentation/processing.

Other concerns of interest surround the response of tumors with low immune infiltration to immunotherapy. Our past work has highlighted the use of radiation to increase immune infiltration into HPV negative immunologically cold tumors in mice, (3). Unfortunately

translating this into the clinic remains difficult as trials with proper controls is lacking. A recent clinical trial involving combination radiation immunotherapy (Nivolumab), although reported as a negative trial, revealed that response rates are different between HPV negative and HPV positive patients with a response rate higher among HPV negative patients (52). However more recent clinical trials such as JAVELIN HN100 have provided negative results suggesting combination radioimmunotherapy will provide no additional benefit (53). Of note, this trial employed elective nodal irradiation, which could have significantly contributed to the blunted immune response. Our past data has shown that the use of FTY720 to prevent egression of T cells from lymph nodes removes the effect of combination radioimmunotherapy (24). Furthermore, the use of conventional radiation fractionation as opposed to hypofractionated SBRT could have contributed to persistent lymphopenia, as we have observed (54). Another pre-clinical study revealed that the sequencing of the immunotherapy with a single high dose of RT can affect systemic immunity, T cell exhaustion, reprogramming, and viability (55). Our observations on the importance of antigen presenting cells in T cell priming and expansion revealed that pulsing the RT is also important for proper immune activation and tumor eradication (24). Within our models, we used two methods of RT, one dose of 10 Gy to treat the LY2 model and fractionated dosing of 8 Gy to treat the MOC2. We have previously established that one dose of 10 Gy in combination with immunotherapy is sufficient for eradication in the LY2 model, but not the MOC2 model in which 5 doses of 8 Gy was required (24). As shown here, in some cases 3 doses of 8 Gy was sufficient for significant tumor growth delay in the MOC2 model. This underscores the importance of the design of preclinical studies in order to better translate them into the clinic.

The data presented here and other recent work suggest that suppression of NK cells within the TME can cripple the immune response, and that therapeutic activation of these populations may provide a method of NK cell-based immunotherapy (56). Our data and other findings discussed here will be critical for rational design of clinical trials aimed at overcoming resistance to radiation and immunotherapy in T-lymphocyte deficient or poorly infiltrated HPV-negative HNSCCs. Adding FLT3L to RT and anti-CD25 therapy led to near eradication of buccal MOC2 tumors. These results are promising for efforts to treat cancers that were previously unresponsive to combination radioimmunotherapies. Our results provide a unique and alternative therapeutic strategy to overcoming resistance to RT and NK cell inactivation through immunotherapeutic approaches targeted directly at the NK cell-DC axis within the TME.

Supplementary Material

Refer to Web version on PubMed Central for supplementary material.

Acknowledgments:

Dr. Sana D. Karam is funded by the NIDCR (R01 DE028529-01, R01 DE028282-01) and receives clinical trial funding from AstraZeneca and preclinical funding from Roche for work unrelated to this research.

References

1. Nör JE, Gutkind JS. Head and Neck Cancer in the New Era of Precision Medicine. J Dent Res (2018) 97:601–602. doi:10.1177/0022034518772278 [PubMed: 29771196]
2. Mandal R, Şenbabaoğlu Y, Desrichard A, Havel JJ, Dalin MG, Riaz N, Lee K-W, Ganly I, Hakimi AA, Chan TA, et al. The head and neck cancer immune landscape and its immunotherapeutic implications. JCI Insight (2016) 1:1–18. doi:10.1172/jci.insight.89829
3. Oweida A, Lennon S, Calame D, Korpela S, Bhatia S, Sharma J, Graham C, Binder D, Serkova N, Raben D, et al. Ionizing radiation sensitizes tumors to PD-L1 immune checkpoint blockade in orthotopic murine head and neck squamous cell carcinoma. Oncoimmunology (2017) 6:1–10.
4. Karam SD, Raben D. Radioimmunotherapy for the treatment of head and neck cancer. Lancet Oncol (2019) 20:e404–e416. doi:10.1016/S1470-2045(19)30306-7 [PubMed: 31364593]
5. Oweida A, Hararah MK, Phan A, Binder D, Bhatia S, Lennon S, Bukkapatnam S, Van Court B, Uyanga N, Darragh L, et al. Resistance to radiotherapy and PD-L1 blockade is mediated by TIM-3 upregulation and regulatory T-cell infiltration. Clin Cancer Res (2018) 24:5368–5380. doi:10.1158/1078-0432.CCR-18-1038 [PubMed: 30042205]
6. Cohen E, Ferris R, Psyrri A. Interim results of the phase III JAVELIN head & neck 100 study in locally advanced squamous cell carcinoma of the head and neck. ESMO Virtual Congr 2020 (2020)
7. Seiwert TY, Burtness B, Mehra R, Weiss J, Berger R, Eder JP, Heath K, McClanahan T, Lunceford J, Gause C, et al. Safety and clinical activity of pembrolizumab for treatment of recurrent or metastatic squamous cell carcinoma of the head and neck (KEYNOTE-012): an open-label, multicentre, phase 1b trial. Lancet Oncol (2016) 17:956–965. doi:10.1016/S1470-2045(16)30066-3 [PubMed: 27247226]
8. Barry KC, Hsu J, Broz ML, Cueto FJ, Binnewies M, Combes AJ, Nelson AE, Loo K, Kumar R, Rosenblum MD, et al. A natural killer–dendritic cell axis defines checkpoint therapy–responsive tumor microenvironments. Nat Med (2018) 24:1178–1191. doi:10.1038/s41591-018-0085-8 [PubMed: 29942093]
9. Clemente-Casares X, Hosseinzadeh S, Barbu I, Dick SA, Macklin JA, Wang Y, Momen A, Kantores C, Aronoff L, Farno M, et al. A CD103+ Conventional Dendritic Cell Surveillance System Prevents Development of Overt Heart Failure during Subclinical Viral Myocarditis. Immunity (2017) 47:974–989.e8. doi:10.1016/j.immuni.2017.10.011 [PubMed: 29166591]
10. Spranger S, Dai D, Horton B, Gajewski TF. Tumor-Residing Batf3 Dendritic Cells Are Required for Effector T Cell Trafficking and Adoptive T Cell Therapy. Cancer Cell (2017) 31:711–723.e4. doi:10.1016/j.ccell.2017.04.003 [PubMed: 28486109]
11. André P, Denis C, Soulas C, Bourbon-Caillet C, Lopez J, Arnoux T, Bléry M, Bonnafous C, Gauthier L, Morel A, et al. Anti-NKG2A mAb Is a Checkpoint Inhibitor that Promotes Anti-tumor Immunity by Unleashing Both T and NK Cells. Cell (2018) 175:1731–1743.e13. doi:10.1016/j.cell.2018.10.014 [PubMed: 30503213]
12. Lucas M, Schachterle W, Oberle K, Aichele P, Diefenbach A. Dendritic Cells Prime Natural Killer Cells by trans-Presenting Interleukin 15. Immunity (2007) 26:503–517. doi:10.1016/j.immuni.2007.03.006 [PubMed: 17398124]
13. Koka R, Burkett P, Chien M, Chai S, Boone DL, Ma A. Cutting Edge: Murine Dendritic Cells Require IL-15Rα to Prime NK Cells. J Immunol (2004) 173:3594–3598. doi:10.4049/jimmunol.173.6.3594 [PubMed: 15356102]
14. Ferlazzo G, Pack M, Thomas D, Paludan C, Schmid D, Strowig T, Bougras G, Muller WA, Moretta L, Münz C. Distinct roles of IL-12 and IL-15 in human natural killer cell activation by dendritic cells from secondary lymphoid organs. Proc Natl Acad Sci U S A (2004) 101:16606–16611. doi:10.1073/pnas.0407522101 [PubMed: 15536127]
15. Abel AM, Yang C, Thakar MS, Malarkannan S. Natural killer cells: Development, maturation, and clinical utilization. Front Immunol (2018) 9:1–23. doi:10.3389/fimmu.2018.01869 [PubMed: 29403488]
16. Guo Y, Luan L, Patil NK, Sherwood ER. Immunobiology of the IL-15 IL-15Rα complex as an antitumor and antiviral agent.pdf. Cytokine and Growth Factor Reveiws (2017) 38:

17. Martrus G, Kautz T, Lunemann S, Richert L, Glau L, Salzberger W, Goebels H, Langeneckert A, Hess L, Poch T, et al. Proliferative capacity exhibited by human liver-resident CD49a+CD25+ NK cells. PLoS One (2017) 12:1–18. doi:10.1371/journal.pone.0182532

18. Martin JF, Perry JSA, Jakhete NR, Wang X, Bielekova B. An IL-2 Paradox: Blocking CD25 on T Cells Induces IL-2–Driven Activation of CD56 bright NK Cells. J Immunol (2010) 185:1311–1320. doi:10.4049/jimmunol.0902238 [PubMed: 20543101]

19. Lee S-H, Fragoso MF, Biron CA. Cutting Edge: A Novel Mechanism Bridging Innate and Adaptive Immunity: IL-12 Induction of CD25 To Form High-Affinity IL-2 Receptors on NK Cells. J Immunol (2012) 189:2712–2716. doi:10.4049/jimmunol.1201528 [PubMed: 22888135]

20. Judd NP, Winkler AE, Murillo-Sauca O, Brotman JJ, Law JH, Lewis JS, Dunn GP, Bui JD, Sunwoo JB, Uppaluri R. ERK1/2 regulation of CD44 modulates oral cancer aggressiveness. Cancer Res (2012) 72:365–374. doi:10.1158/0008-5472.CAN-11-1831 [PubMed: 22086849]

21. Chen Z, Smith CW, Kiel D, Van Waes C. Metastastic variants derived following in vivo tumor progression of an in vitro transformed squamous cell carcinoma line acquire a differential growth advantage requiring tumor-host interaction. Clin Exp Metastasis (1997) 15:527–537. doi:10.1023/A:1018474910432 [PubMed: 9247255]

22. Lahl K, Loddenkemper C, Drouin C, Freyer J, Arnason J, Eberl G, Hamann A, Wagner H, Huehn J, Sparwasser T. Selective depletion of Foxp3+ regulatory T cells induces a scurfy-like disease. J Exp Med (2007) 204:57–63. doi:10.1084/jem.20061852 [PubMed: 17200412]

23. Hildner K, Edelson BT, Purtha WE, Diamond M, Matsushita H, Kohyama M, Calderon B, Schraml BU, Unanue ER, Diamond MS, et al. Batf3 deficiency reveals a critical role for CD8α + dendritic cells in cytotoxic T cell immunity. Science (80-) (2008) 322:1097–1100. doi:10.1126/science.1164206

24. Knitz MW, Bickett TE, Darragh LB, Oweida AJ, Bhatia S, Van Court B, Bhuvane S, Piper M, Gadwa J, Mueller AC, et al. Targeting resistance to radiation-immunotherapy in cold HNSCCs by modulating the Treg-dendritic cell axis. J Immunother cancer (2021) 9: doi:10.1136/jitc-2020-001955

25. Lahl K, Sparwasser T. In Vivo Depletion of FoxP3+ Tregs Using the DEREG Mouse Model. Methods Mol Biol (2011)157–172.

26. Petit V, Massonnet G, MacIorowski Z, Touhami J, Thuleau A, Némati F, Laval J, Château-Joubert S, Servely JL, Vallerand D, et al. Optimization of tumor xenograft dissociation for the profiling of cell surface markers and nutrient transporters. Lab Investig (2013) 93:611–621. doi:10.1038/labinvest.2013.44 [PubMed: 23459372]

27. Van Gassen S, Callebaut B, Van Helden MJ, Lambrecht BN, Demeester P, Dhaene T, Saeys Y. FlowSOM : Using Self-Organizing Maps for Visualization and Interpretation of Cytometry Data. Cytometry (2015) 87A:636–645. doi:10.1002/cyto.a.22625

28. Somanchi SS, McCulley KJ, Somanchi A, Chan LL, Lee DA. A novel method for assessment of natural killer cell cytotoxicity using image cytometry. PLoS One (2015) 10:1–15. doi:10.1371/journal.pone.0141074

29. Biswas BK, Guru SA, Sumi MP, Jamatia E, Gupta RK, Lali P, Konar BC, Saxena A, Mir R. Natural killer cells expanded and preactivated exhibit enhanced antitumor activity against different tumor cells in vitro. Asian Pacific J Cancer Prev (2020) 21:1595–1605. doi:10.31557/APJCP.2020.21.6.1595

30. An IL-15 superagonist IL-15Rα fusion complex protects and rescues NK cell cytotoxic function from TGF b1 mediated immunosuppresion.pdf.

31. Sergushichev A An algorithm for fast preranked gene set enrichment analysis using cumulative statistic calculation. bioRxiv (2016) Available at: https://www.biorxiv.org/content/biorxiv/early/2016/06/20/060012.full.pdf

32. Kanehisa M, Goto S. KEGG: Kyoto Encyclopedia of Genes and Genomes. Nuclic Acids Res (2000) 28:27–30. doi:10.3892/ol.2020.11439

33. Korrer MJ, Kim YJ. Natural Killer cells from primary human head and neck squamous cell carcinomas upregulate NKG2A. J Immunol (2017) 198:

34. Ravetch JV, Lanier LL. Immune inhibitory receptors. Science (80-) (2000) 290:84–89. doi:10.1126/science.290.5489.84

35. Chiossone L, Chaix J, Fuseri N, Roth C, Vivier E, Walzer T. Maturation of mouse NK cells is a 4-stage developmental program. Blood (2009) 113:5488–5496. doi:10.1182/blood-2008-10-187179 [PubMed: 19234143]
36. Xu D, Gu P, Pan PY, Li Q, Sato AI, Chen SH. NK and CD8 + T cell-mediated eradication of poorly immunogenic B16-F10 melanoma by the combined action of IL-12 gene therapy and 4-1BB costimulation. Int J Cancer (2004) 109:499–506. doi:10.1002/ijc.11696 [PubMed: 14991570]
37. Eidenschenk C, Crozat K, Krebs P, Arens R, Popkin D, Arnold CN, Blasius AL, Benedict CA, Moresco EMY, Xia Y, et al. Flt3 permits survival during infection by rendering dendritic cells competent to activate NK cells. Proc Natl Acad Sci (2010) 107:9759–9764. doi:10.1073/pnas.1005186107 [PubMed: 20457904]
38. Oweida AJ, Darragh L, Phan A, Binder D, Bhatia S, Mueller A, Van Court B, Milner D, Raben D, Woessner R, et al. STAT3 Modulation of Regulatory T Cells in Response to Radiation Therapy in Head and Neck Cancer. JNCI J Natl Cancer Inst (2019) 111:6–10. doi:10.1093/jnci/djz036
39. Salmon H, Idoyaga J, Rahman A, Leboeuf M, Remark R, Jordan S, Casanova-Acebes M, Khudoynazarova M, Agudo J, Tung N, et al. Expansion and Activation of CD103+ Dendritic Cell Progenitors at the Tumor Site Enhances Tumor Responses to Therapeutic PD-L1 and BRAF Inhibition. Immunity (2016) 44:924–938. doi:10.1016/j.immuni.2016.03.012 [PubMed: 27096321]
40. Dong W, Wu X, Ma S, Wang Y, Nalin AP, Zhu Z, Zhang J, Benson DM, He K, Caligiuri MA, et al. The mechanism of anti–pd-l1 antibody efficacy against pd-l1–negative tumors identifies nk cells expressing pd-l1 as a cytolytic effector. Cancer Discov (2019) 9:1422–1437. doi:10.1158/2159-8290.CD-18-1259 [PubMed: 31340937]
41. Chiossone L, Dumas PY, Vienne M, Vivier E. Natural killer cells and other innate lymphoid cells in cancer. Nat Rev Immunol (2018) 18:671–688. doi:10.1038/s41577-018-0061-z [PubMed: 30209347]
42. Létourneau S, Krieg C, Pantaleo G, Boyman O. IL-2- and CD25-dependent immunoregulatory mechanisms in the homeostasis of T-cell subsets. J Allergy Clin Immunol (2009) 123:758–762. doi:10.1016/j.jaci.2009.02.011 [PubMed: 19348914]
43. Stoklasek TA, Schluns KS, Lefrançois L. Combined IL-15/IL-15Rα Immunotherapy Maximizes IL-15 Activity In Vivo. J Immunol (2006) 177:6072–6080. doi:10.4049/jimmunol.177.9.6072 [PubMed: 17056533]
44. Rubinstein MP, Kovar M, Purton JF, Cho JH, Boyman O, Surh CD, Sprent J. Converting IL-15 to a superagonist by binding to soluble IL-15Rα. Proc Natl Acad Sci U S A (2006) 103:9166–9171. doi:10.1073/pnas.0600240103 [PubMed: 16757567]
45. Hémar A, Subtil A, Lieb M, Morelon E, Hellio R, Dautry-Varsat A. Endocytosis of interleukin 2 receptors in human T lymphocytes: Distinct intracellular localization and fate of the receptor α, β, and γ chains. J Cell Biol (1995) 129:55–64. doi:10.1083/jcb.129.1.55 [PubMed: 7698995]
46. Loyon R, Picard E, Mauvais O, Queiroz L, Mougey V, Pallandre J-R, Galaine J, Mercier-Letondal P, Kellerman G, Chaput N, et al. IL-21–Induced MHC Class II + NK Cells Promote the Expansion of Human Uncommitted CD4 + Central Memory T Cells in a Macrophage Migration Inhibitory Factor–Dependent Manner. J Immunol (2016) 197:85–96. doi:10.4049/jimmunol.1501147 [PubMed: 27233967]
47. Crome SQ, Lang PA, Lang KS, Ohashi PS. Natural killer cells regulate diverse T cell responses. Trends Immunol (2013) 34:342–349. doi:10.1016/j.it.2013.03.002 [PubMed: 23601842]
48. Cho JH, Boyman O, Kim HO, Hahm B, Rubinstein MP, Ramsey C, Kim DM, Surh CD, Sprent J. An intense form of homeostatic proliferation of naive CD8+ cells driven by IL-2. J Exp Med (2007) 204:1787–1801. doi:10.1084/jem.20070740 [PubMed: 17664294]
49. Bielekova B, Catalfamo M, Reichert-Scrivner S, Packer A, Cerna M, Waldmann TA, McFarland H, Henkart PA, Martin R. Regulatory CD56bright natural killer cells mediate immunomodulatory effects of IL-2Rα-targeted therapy (daclizumab) in multiple sclerosis. Proc Natl Acad Sci U S A (2006) 103:5941–5946. doi:10.1073/pnas.0601335103 [PubMed: 16585503]
50. Wisdom AJ, Mowery YM, Hong CS, Himes JE, Nabet BY, Qin X, Zhang D, Chen L, Fradin H, Patel R, et al. Single cell analysis reveals distinct immune landscapes in transplant and primary sarcomas that determine response or resistance to immunotherapy. Nat Commun (2020) 11: doi:10.1038/s41467-020-19917-0

51. Crittenden MR, Zebertavage L, Kramer G, Bambina S, Friedman D, Troesch V, Blair T, Baird JR, Alice A, Gough MJ. Tumor cure by radiation therapy and checkpoint inhibitors depends on pre-existing immunity. Sci Rep (2018) 8:1–15. doi:10.1038/s41598-018-25482-w [PubMed: 29311619]

52. McBride S, Sherman E, Tsai CJ, Baxi S, Aghalar J, Eng J, Zhi WI, McFarland D, Michel LS, Young R, et al. Randomized Phase II Trial of Nivolumab With Stereotactic Body Radiotherapy Versus Nivolumab Alone in Metastatic Head and Neck Squamous Cell Carcinoma. J Clin Oncol (2021) 39:30–37. [PubMed: 32822275]

53. Lee NY, Ferris RL, Psyrri A, Haddad RI, Tahara M, Bourhis J, Harrington K, Chang PMH, Lin JC, Razaq MA, et al. Avelumab plus standard-of-care chemoradiotherapy versus chemoradiotherapy alone in patients with locally advanced squamous cell carcinoma of the head and neck: a randomised, double-blind, placebo-controlled, multicentre, phase 3 trial. Lancet Oncol (2021) 22:450–462. doi:10.1016/S1470-2045(20)30737-3 [PubMed: 33794205]

54. Sumner WA, Stokes WA, Oweida A, Berggren KL, McDermott JD, Raben D, Abbott D, Jones B, Gan G, Karam SD. Survival impact of pre-treatment neutrophils on oropharyngeal and laryngeal cancer patients undergoing definitive radiotherapy. J Transl Med (2017) 15:1–9. doi:10.1186/s12967-017-1268-7 [PubMed: 28049494]

55. Wei J, Montalvo-Ortiz W, Yu L, Krasco A, Ebstein S, Cortez C, Lowy I, Murphy AJ, Sleeman MA, Skokos D. Sequence of αPD-1 relative to local tumor irradiation determines the induction of abscopal antitumor immune responses. Sci Immunol (2021) 6: doi:10.1126/sciimmunol.abg0117

56. Neo SY, Yang Y, Record J, Ma R, Chen X, Chen Z, Tobin NP, Blake E, Seitz C, Thomas R, et al. CD73 immune checkpoint defines regulatory NK cells within the tumor microenvironment. J Clin Invest (2020) 130:1185–1198. doi:10.1172/JCI128895 [PubMed: 31770109]

Statement of translational relevance

HPV negative head and neck squamous cell carcinoma (HNSCC) are immunologically cold tumors that have shown limited response to treatment. Although radiation therapy (RT) is a mainstay treatment for this cancer, resistance develops, even in combination with immune checkpoint inhibitors. The dendritic cell growth factor FLT3L has shown success in treating other cancers and here we detail the important role it plays in overcoming resistance to radiation therapy in HNSCC. We show that NK cells' secretion of FLT3L is essential for response to radio-immunotherapy. However, neither doublet combination of anti-NKG2A with RT nor FLT3L agonist with RT results in tumor growth delay. Depending on the model, overcoming regulatory T cells (Tregs) immunosuppressive function with or without dendritic cell agonists, such as anti-CD137, is essential to achieve meaningful tumor growth delay or eradication, a response that requires NK cells. We identify consumption of IL2 by Tregs, and its blockade with antiCD25, as a major mechanism mediating NK cell function, whereby IL-2 stimulates NK cells through CD122. In a field where the majority of radio-immunotherapy trials are failing, these data stand to provide rational design for educating clinical trial translation in HNSCC.

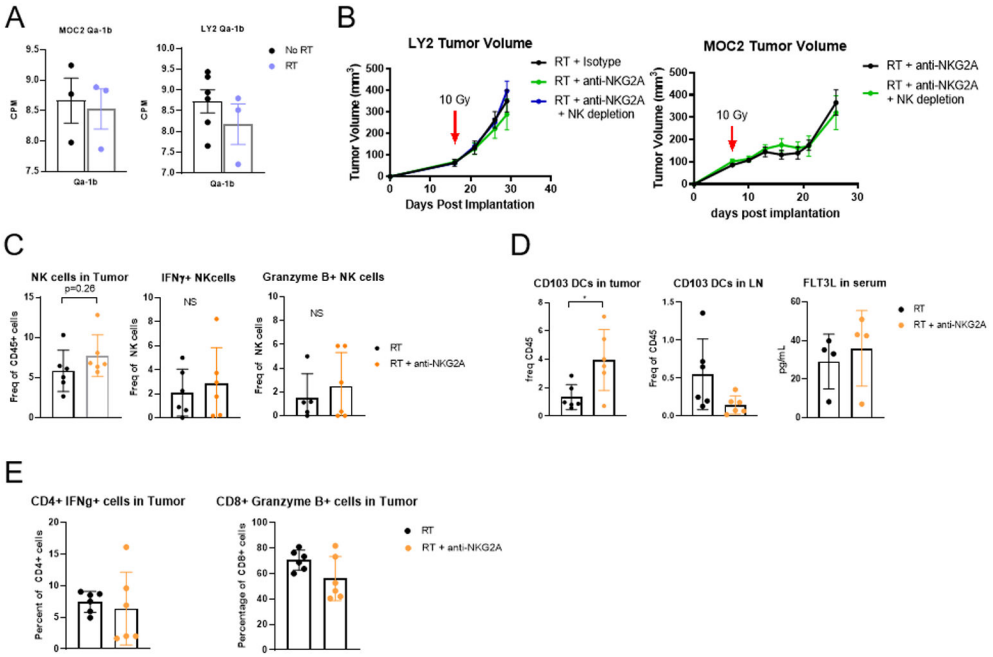

Figure 1.

(A) Bulk RNAseq data from MOC2 and LY2 tumors showing the expression levels of Qa-1b 7 days after RT in the MOC2 model and 10 days after RT in the LY2 model; n=4. (B) Tumor volumes in mice bearing MOC2 and Ly2 tumors treated with RT and anti-NKG2A and either depleted or not depleted of NK cells; n=7. (C) Flow Cytometric analysis of NK cell populations in MOC2 tumors 3 days after RT and anti-NKG2A therapy shown as frequency of parent population; n=6. (D) Flow Cytometric analysis of DC populations in MOC2 tumors and ELISA analysis of FLT3L levels in serum 3 days after RT and anti-NKG2A therapy; n=6. (E) Flow Cytometric analysis of effector T cell populations in MOC2 tumors 3 days after RT and anti-NKG2A therapy; n=6.

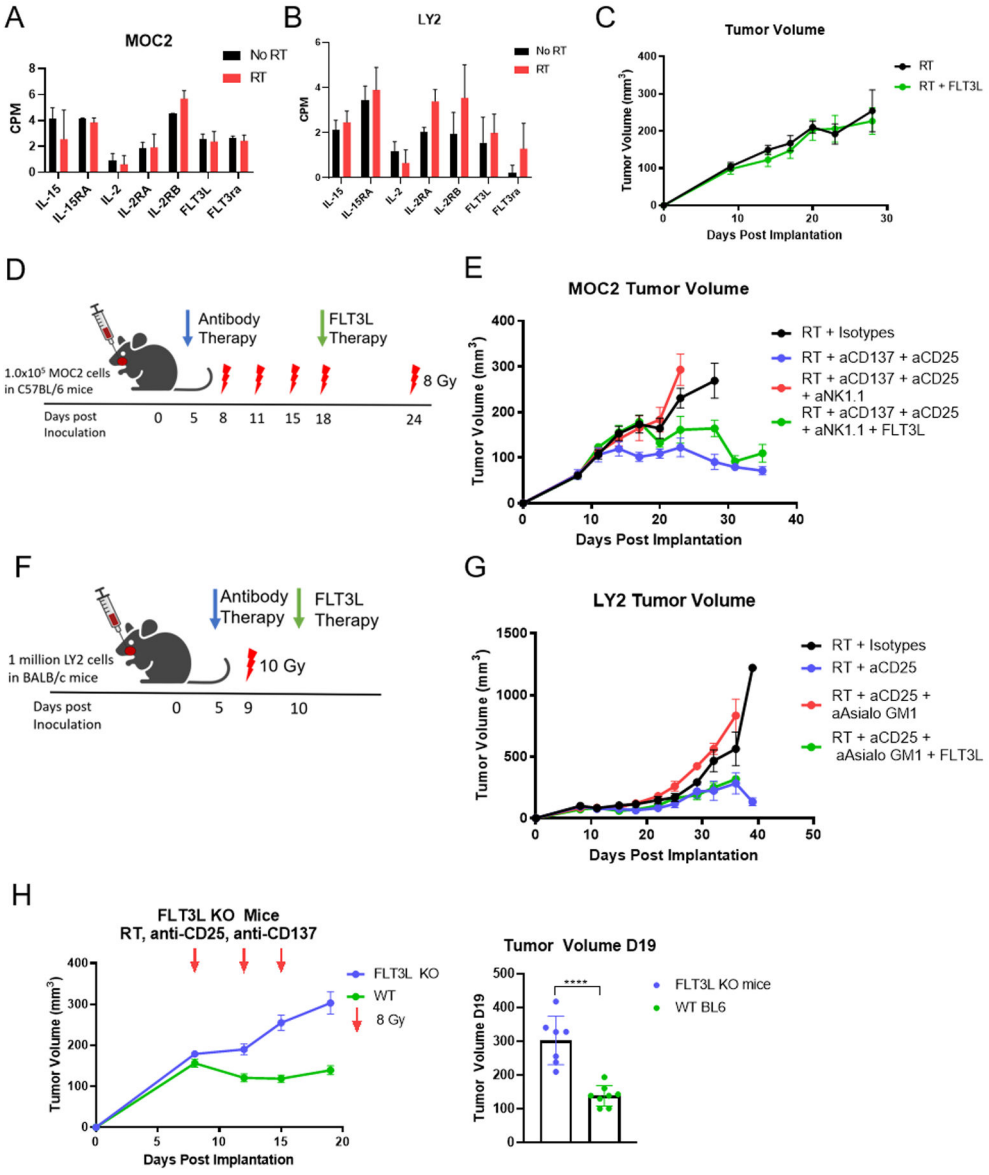

Figure 2.

(A) Bulk RNAseq analysis of MOC2 tumors showing IL-15, IL-15RA, IL-2, IL-2RA, IL-2RB, FLT3L, and FLT3RA production in MOC2 tumors 7 days after RT; n=4. (B) Bulk RNAseq analysis of LY2 tumors showing IL-15, IL-15RA, IL-2, IL-2RA, IL-2RB, FLT3L, and FLT3RA production in LY2 tumors 10 days after RT; n=4. (C) MOC2 tumor volumes of mice treated with RT (8 Gy) on days 9, 18, and 22 with FLT3L HDT therapy starting on day 11; n=7. (D) Schematic of MOC2 experiment in C57BL/6 mice depicts days of 8 Gy RT (red lightning bolts), beginning of antibody therapy at day 4 (blue arrow), and FLT3L therapy at day 18 (i.p. injection daily for 10 days) (green arrow); n=7. (E) MOC2 tumor volumes of C57BL/6 mice treated with RT and isotype control (black line), anti-CD137 and anti-CD25 (blue line), anti-CD137 and anti-CD25 with NK cells depleted (red line), and anti-CD137 and anti-CD25 with NK cells depleted plus FLT3L therapy (green line); n=7. (F) Schematic of LY2 experiment in BALB/c mice depicts 10 Gy of RT at day 9 (red

lightning bolt), beginning of antibody therapy at day 5 (blue arrow), and FLT3L therapy at day 10 (Hydrodynamic injection) (green arrow). (G) LY2 tumor volumes of BALB/c mice after treatment with RT and isotypes (black line), anti-CD25 (blue line), anti-CD25 with NK cells depleted (red line), anti-CD25 with NK cells depleted plus FLT3L HDT therapy (green line); n=7. (H) Tumor volumes on days 6, 12, 15, 19 (*left panel*) and on day 19 (*right panel*) in wild type C57BL/6 (green line) and FLT3L knockout (blue symbols) mice treated twice weekly with RT + anti-CD25 + anti-CD137 and 8 Gy buccal irradiation on days 8, 12, and 15; ****$p \leq 0.0001$; n=7.

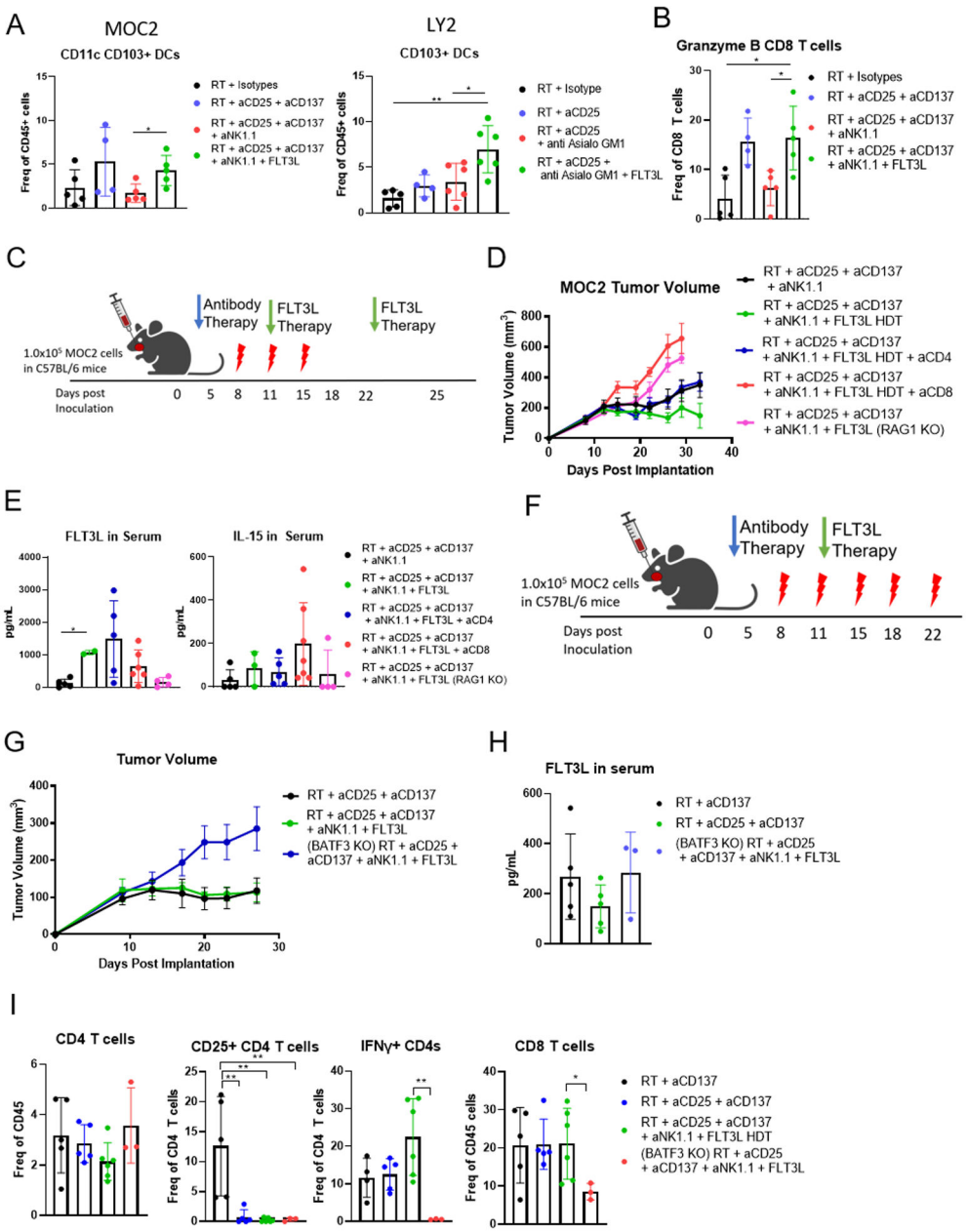

Figure 3.

(A) Flow Cytometric analysis of CD103^{+} DC populations in MOC2 and LY2 tumors. MOC2 tumors were taken 3 days after RT, NK cell depletion, and FLT3L therapy. LY2 tumors were taken 9 days post RT, anti-CD25, and FLT3L HDT; *p≤0.1 **p≤0.05 n=6. (B) Flow Cytometric analysis of CD8 T cell populations in MOC2 tumors 24 days after RT and 10 days after the start of FLT3L therapy; *p≤0.1, **p≤0.05; n=5. (C) Schematic of experimental procedure for CD4 and CD8 T cell depletion in C57BL/6 mice bearing MOC2 tumors depicts days of administration of 8 Gy RT (red lightning bolt), beginning of antibody therapy (blue arrow), and FLT3L HDT therapy (green arrow). (D) MOC2 Tumor volumes of C57BL/6 and RAG$^{-/-}$ mice treated with RT, anti-CD25, anti-CD137, and depleted of

NK cells (black line), treated with FLT3L HDT therapy (green line) and depleted of CD4 T cells (blue line), CD8 T cells (red line), and $RAG^{-/-}$ mice devoid of CD4 and CD8 T cells (pink line); n=7. (E) FLT3L and IL-15 levels in serum of T cell-depleted (ELISA); n=6. (F) Schematic of experimental procedure involving WT C57BL/6 and $BATF3^{-/-}$ mice to be treated with RT, anti-CD25, anti-CD137, depleted of NK cells, and FLT3L HDT therapy depicts days of RT (red lightning bolt), beginning of antibody therapy (blue arrow), and FLT3L HDT therapy (green arrow). (G) MOC2 tumor volumes of WT C57BL/6 mice treated with RT, anti-CD25, and anti-CD137 (black line), NK cell depletion and FLT3L HDT therapy (green line), and $BATF3^{-/-}$ mice treated with RT, anti-CD25, anti-CD137, NK cell depletion, and FLT3L HDT therapy (blue line); n=7. (H) FLT3L serum levels (ELISA) in WT C57BL/6 mice and $BATF3^{-/-}$ mice treated with RT, anti-CD25, anti-CD137, NK cell depletion, and FLT3L HDT therapy; N=5. (I) Flow cytometric analysis of CD4 and CD8 T cell populations in tumors of WT C57BL/6 mice and $BATF3^{-/-}$ mice treated with RT, anti-CD137, anti-CD25, NK cell depletion, and FLT3L HDT therapy; n=5.

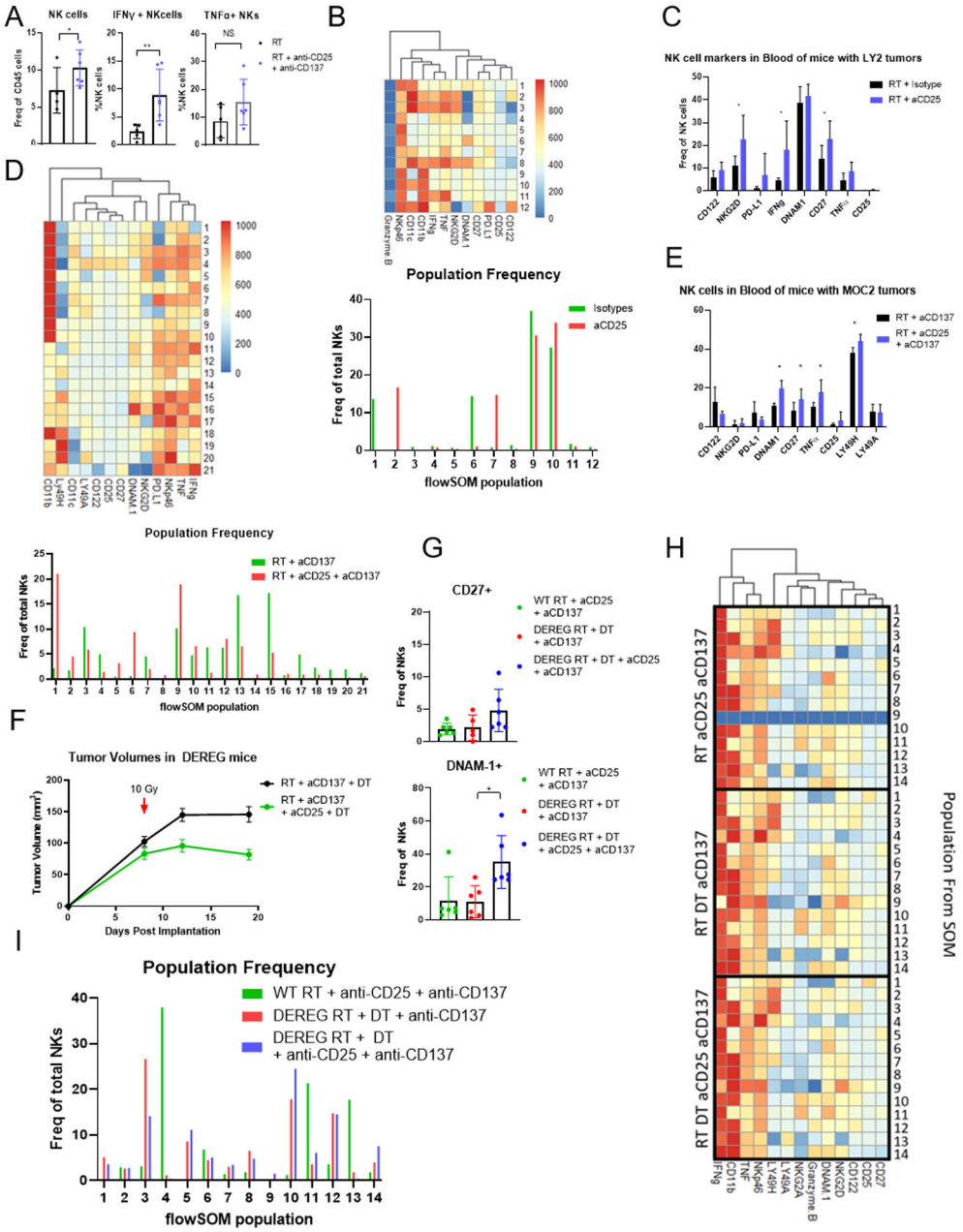

Figure 4.

(A) Flow Cytometric analysis of NK cell populations in MOC2 tumors 3 days after start of treatment with 10 Gy RT, anti-CD25, anti-CD137, compared to RT alone.; *p≤0.1, **p≤0.05; n=5. (B) FlowSOM clustering of raw flow cytometry of NK cell populations in LY2 tumors treated with 10 Gy RT and either isotype antibody or anti-CD25 antibody. Tumors were taken 8 days after RT; *p≤0.1, **p≤0.05; n=5. (C) Flow Cytometry of NK cells in blood of LY2 tumor-bearing BALB/c mice taken 8 days after 10 Gy RT; *p≤0.1, **p≤0.05; n=5. (D) FlowSOM clustering of raw flow cytometry of NK cell populations in MOC2 tumors treated with 10 Gy RT and anti-CD137 antibody with and without anti-CD25 antibody. Tumors were taken 13 days after RT; *p≤0.05; n=5. (E) Flow cytometry

of NK cells in blood of MOC2-bearing C57BL/6 mice taken 13 days after 10 gy RT; *p≤0.05; n=5. (F) Tumor volumes of MOC2 tumors from DEREG mice treated with 10 Gy RT, anti-CD137, and diphtheria toxin (DT) (black line) or treated with RT, anti-CD25, anti-CD137, and diphtheria toxin (DT) (green line); n=7. (G) Flow cytometry of NK cell populations in blood from WT C57BL/6 mice treated with 10 Gy RT, anti-CD25, and anti-CD137 and from DEREG mice treated with 10 Gy RT, anti-CD25, anti-CD137, and diphtheria toxin (DT); *p≤0.05; n=5. (H) Heatmap depicting the 14 populations of NK cells identified by FlowSOM, and the relative expression of markers of those populations in WT C57BL/6 mice treated with RT, anti-CD25, and anti-CD137 and in DEREG mice treated with RT, anti-CD137, and diphtheria toxin (DT) or treated with 10 Gy RT, anti-CD25, anti-CD137, and diphtheria toxin (DT); n=5. (I) Frequency of populations identified by FlowSOM in C57BL/6 mice treated with 10 Gy RT, anti-CD25, and anti-CD137 and in DEREG mice treated with 10 Gy RT, anti-CD137, and diphtheria toxin (DT) or treated with RT, anti-CD25, anti-CD137, and diphtheria toxin (DT); n=5.

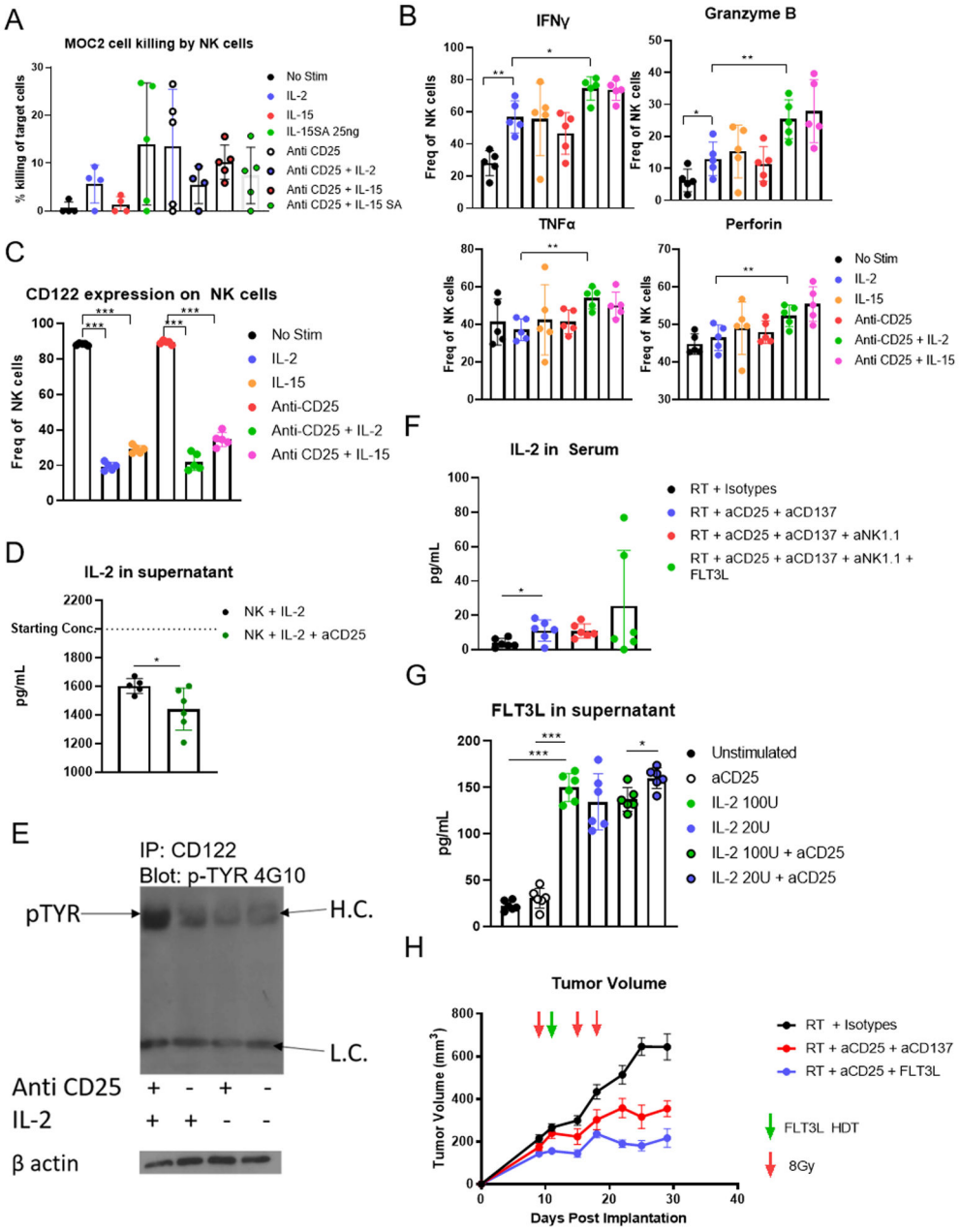

Figure 5.

(A) Percent killing of MOC2 tumor cells *in vitro* by NK cells harvested from the spleens of C57BL/6 mice by negative selection; n=5. (B) Flow cytometric analysis of in vitro NK cell populations; *p≤0.05, **p≤0.01; n=5. (C) Expression of CD122 and IL-2RB on NK cells treated *in vitro*; n=5. (D) Quantitation of IL-2 in the supernatant of isolated NK cells stimulated with or without anti-CD25; n=6. (E) Western blot of immunoprecipitated CD122 probed with anti-phosphotyrosine. CD122 was immunoprecipitated from NK cells isolated from C57BL/6 mice and stimulated with anti-CD25 and IL-2 as indicated. (F) Concentrations of IL-2 in serum of C57BL/6 mice; *p≤0.05; n=6. (G) Concentration of FLT3L in the supernatant of NK cells stimulated with exogenous IL-2 (ELISA) as indicated;

*p≤0.05, ***p≤0.001; n=6. (H) Volumes of MOC2 tumors in mice treated with RT, anti-CD25, anti-CD137, and FLT3L hydrodynamic delivery; n=7.

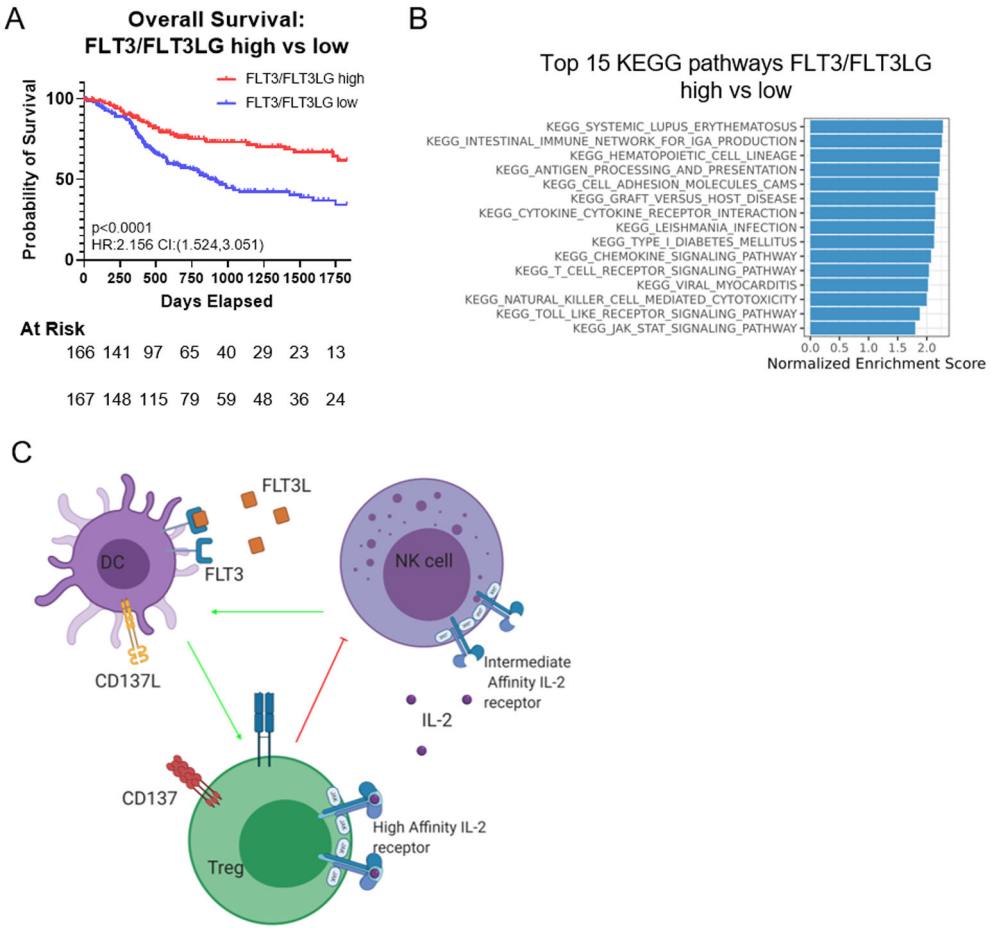

Figure 6.

(A) Overall survival of patients with high expression of both FLT3LG and FLT3 to patients with low expression of FLT3LG/FLT3. (B) Waterfall plot showing KEGG pathways upregulated in patients with high expression of both FLT3 and FLT3LG. all pathways displayed are top 15 pathways and have calculated adjusted p<0.001 as generated by fgsea. (C) Schematic depicting the interaction between NK cells, DCs, and Tregs in the TME and the cytokines that govern their interactions. In both the LY2 and MOC2 models NK cells are key, as the effect of therapy is removed upon their depletion, and can be rescued by FLT3L therapy. NK cells can be stimulated by IL-2, and play a critical role in producing FLT3L to activate DCs. DCs, once activated by FLT3L, increase tumor surveillance and T cell activation. Tregs play a negative role through IL-2 sequestration.